LA-UR- 11-02843

Approved for public release; distribution is unlimited.

Title:	X-Ray Fluorescence for Safeguards of Spent Fuel Assemblies
Author(s):	C. R. Freeman V. Mozin S. J. Tobin M. L. Fensin W. S. Charlton H. R. Trellue J. D. Galloway
Intended for:	ESARDA conference, Budapest, Hungary, May 16-20, 2011

Los Alamos
NATIONAL LABORATORY
EST. 1943

Form 836 (7/06)

X-Ray Fluorescence for Safeguards of Spent Fuel Assemblies

C. Freeman[1], V. Mozin[1,2,3], S. Tobin[1], M. Fensin[1], W. Charlton[4], H. Trellue[1], J. Galloway[1]

[1]Los Alamos National Laboratory
[2]University of California at Berkeley
[3]Lawrence Berkeley National Laboratory
[4]Texas A&M University
Email: coreyf@lanl.gov

Abstract:

Quantifying the plutonium (Pu) content in spent fuel is necessary for many reasons, particularly to verify that diversion or other illicit activities have not occurred. The Next Generation Safeguards Initiative (NGSI) is funding a large collaborative effort between multiple laboratories and universities to improve spent nuclear fuel safeguards methods and equipment. This effort involves the current work of modeling several different nondestructive assay (NDA) techniques. We expect that the best solution, given the safeguard need, will involve combining a few instruments into a system. The insights gained from this research will be used to down-select a few of the most promising techniques that complement each other from the original set. The goal is to integrate the selected instruments together to create an accurate measurement system for fuel verification that is also robust enough to detect diversions. These instruments will then be, fabricated and tested. This work examines one of the NDA techniques—measuring x-ray emission peaks from Pu and uranium (U) to gather information about their relative quantities in a spent fuel assembly. X-ray fluorescence (XRF) is unique among the techniques in that it is the only one able to give the ratio of elemental Pu/U, allowing the Pu mass to be quantified for the assembly if U is known. XRF also presents many challenges, such as penetration issues because the low energy x-rays desired are effectively shielded by the first few millimeters of a fuel pin. This paper explores the capability of the Monte Carlo N-Particle eXtended (MCNPX) transport code to predict XRF measurements of spent fuel rods made at Oak Ridge National Laboratory (ORNL). MCNPX is then used to simulate detected x-ray peaks for a suite of modeled spent fuel assemblies with various burnups (BUs), initial ^{235}U enrichments (IEs), and cooling times (CTs). Analysis of XRF feasibility for safeguards of spent nuclear fuel assemblies will be discussed.

Keywords: X-Ray; Fluorescence; Spent Fuel; NDA;

1. Introduction

The U.S. Department of Energy (DOE) through the Next Generation Safeguards Initiative (NGSI) of NA-24 is funding a large collaborative effR. ort between multiple laboratories and universities to improve spent nuclear fuel safeguards methods and equipment [1].This effort involves the current work of modeling several different nondestructive assay (NDA) techniques. Several approaches are being researched since we expect that the safeguard need will best be met by combining the attributes from a few NDA techniques [2]. The understanding gained from this effort will be used to down-select to a few of the most promising techniques that complement each other most effectively. The goal is to integrate the selected instruments together to create an accurate measurement system for fuel verification that can also detect diversions. These instruments will be fabricated and tested to directly demonstrate fitness for purpose.

The work presented here focuses on the feasibility of using x-ray fluorescence (XRF) as a tool to quantify the elemental abundance of plutonium (Pu) in pressurized water reactor (PWR) spent fuel assemblies. XRF is unique among the other techniques being explored in that it offers the ability to measure the elemental quantity of Pu, as opposed to isotopic properties. Given that our motivation is to apply XRF to assemblies, recent XRF measurements of single spent fuel pins provide an opportunity to build confidence that XRF modeling capabilities can accurately predict the x-ray signal from spent fuel. Therefore, the first task will be to attempt to simulate pin measurements, compare to measured data, and then simulations will examine the feasibility of the XRF technique on assemblies.

1.1 Background

When an electron is freed from the inner orbit of an atom, an electron from a less tightly bound orbit transitions to the inner orbit to fill the vacancy. The difference in binding energy between the two orbits is released as an x-ray with high probability. The energy of the x-rays is characteristic of the element. Therefore, measuring the ratio of uranium (U) and Pu x-ray peaks provides information about the relative concentration of U and Pu present in the sample. If the total mass of U is accurately known, then the total mass of Pu can be calculated. There are many means by which an atom can become ionized in spent fuel. The two main sources of excitation energy, those considered in this work, are gamma rays and beta particles, both of which have a high passive flux inside the irradiated fuel arising from the decay of fission fragments. The energies of x-rays for Pu and U for the most intense peaks (K_α and K_β) are shown in Table 1 [3]. The most intense $K_{\alpha 1}$ x-rays are used for the Pu / U ratio.

	Levels	Energy [keV]		Relative Intensity	
X Ray	(Final - Initial)	Uranium	Plutonium	Uranium	Plutonium
$K_{\alpha 2}$	$K - L_2$	94.67	99.55	61.9	62.5
$K_{\alpha 1}$	$K - L_3$	98.44	103.76	100	100
$K_{\beta 1}$	$K - M_3$	111.3	117.26	22	22.2
$K_{\beta 2}$	$K - N_{2-5}$	114.5	120.6	12.3	12.5
$K_{\beta 3}$	$K - M_2$	110.41	116.27	11.6	11.7

Table 1: Energies and relative intensity of major x-rays for U and Pu.

1.2 Measuring XRF

Photon measurements of spent fuel using high resolution spectrometers exhibit a large background continuum in the low energy x-ray region due to Compton scattering of the intense energetic gamma photons created by spent fuel. The high Compton continuum can make x-ray measurements of the less abundant Pu difficult because of the relatively small signal-to-background ratio produced. In typical PWRs, only 1 to 2% of the spent fuel is Pu by weight. In lower burnup (BU) fuels with less Pu, the signal-to-background of the Pu x-ray peak may be too small for accurate and timely measurements. Few attempts have been made in the past to measure the Pu x-rays in spent nuclear fuel, [4] but recent measurement campaigns demonstrate Pu x-rays for PWR spent fuel pins with BUs ranging from 35 to 70 Gwd/tU can be measured [5]. One of the challenges XRF faces is a mean free path in nuclear fuel of ~0.5 mm. Therefore, only the outer layer of a fuel pin is really being measured. Furthermore, the high photon flux created by spent fuel means that long collimators are needed to keep count rates within detector limitations. In addition, because of the low signal-to-background of the Pu x ray, long count times are needed per detector; hence, it is necessary to use multiple detectors in order to achieve reasonable count times.

2. North Anna Fuel Pin Measurements

XRF experimental measurement campaigns of spent fuel were undertaken at Oak Ridge National Laboratory (ORNL) in May 2008, July 2008, and January 2009. Fuel pins from North Anna and Three Mile

Island were measured at various axial positions along the fuel rod to get a range of BUs. Data were collected using both coaxial and planar high purity germanium (HPGe) detectors to cover a wide range of energies with high resolution. The coaxial detector would be typical of the kind used for BU determination, but the thinner planar detector offers better signal-to-background for x-ray energies due to the low efficiency for higher energy gammas.

This section focuses on measurements of a North Anna fuel pin nominally burned to ~67 Gwd/tU, 4.7 years cooling time (CT), with 4.2% initial enrichment, which is used for comparison to Monte Carlo N-Particle eXtended (MCNPX) computational models [6]. While measurements are currently only available for single fuel pins, the ultimate goal of this project is to determine the capabilities of XRF to efficiently measure entire assemblies. As the first step to that end, modeling efforts are benchmarked against the ORNL fuel pin measurements. The North Anna fuel pin measurements were selected because of the high BU, and thus high Pu content; therefore, the benchmarked case represents the best case scenario.

2.1 XRF Experiment

The North Anna fuel pin, labeled 649, was cut axially into smaller pieces. The pin piece, labeled 649C, was cut far enough away from the ends that the axial Pu profile would be flat. 649C was wrapped in a stainless steel shipping tube with walls 1/16th of an inch thick (0.15875 cm). The pin piece was positioned inside a hot cell, and a planar HPGe detector was placed outside the hot cell at the end of a stainless steel collimator that penetrates through a concrete wall. The detector was ~120 cm from the center of the fuel pin. The collimator was ~90 cm long, with a 0.2 cm diameter hole. The collimator hole is not concentric with the collimator, which is 2.4 cm thick at the narrowest point. Figure 1 illustrates the experimental setup. Multiple measurements were taken with the planar detector using a count time of 1 hour, in which Pu x-ray peaks were visible. An overnight spectrum was also taken to improve statistical precision. Figure 2 shows the overnight spectrum of the North Anna fuel pin 649C taken at ORNL. The U x-ray peaks are clearly visible above the Compton background. A challenge of XRF for spent fuel is the relatively small number of counts in the Pu $K_{\alpha 1}$ peak. Fortunately, the continuum in the background region is fairly level.

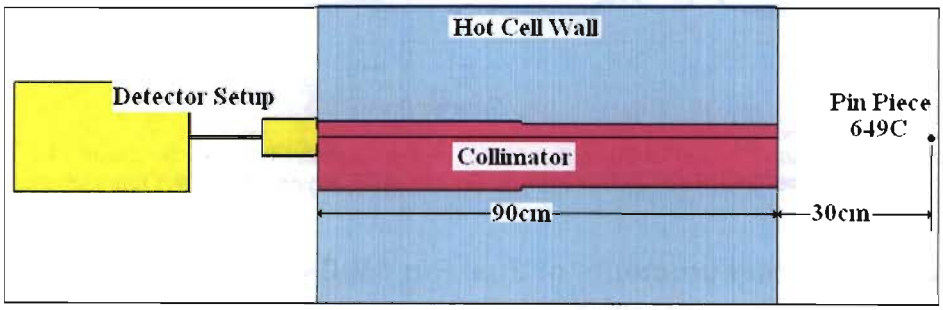

Figure 1: Schematic of experimental setup.

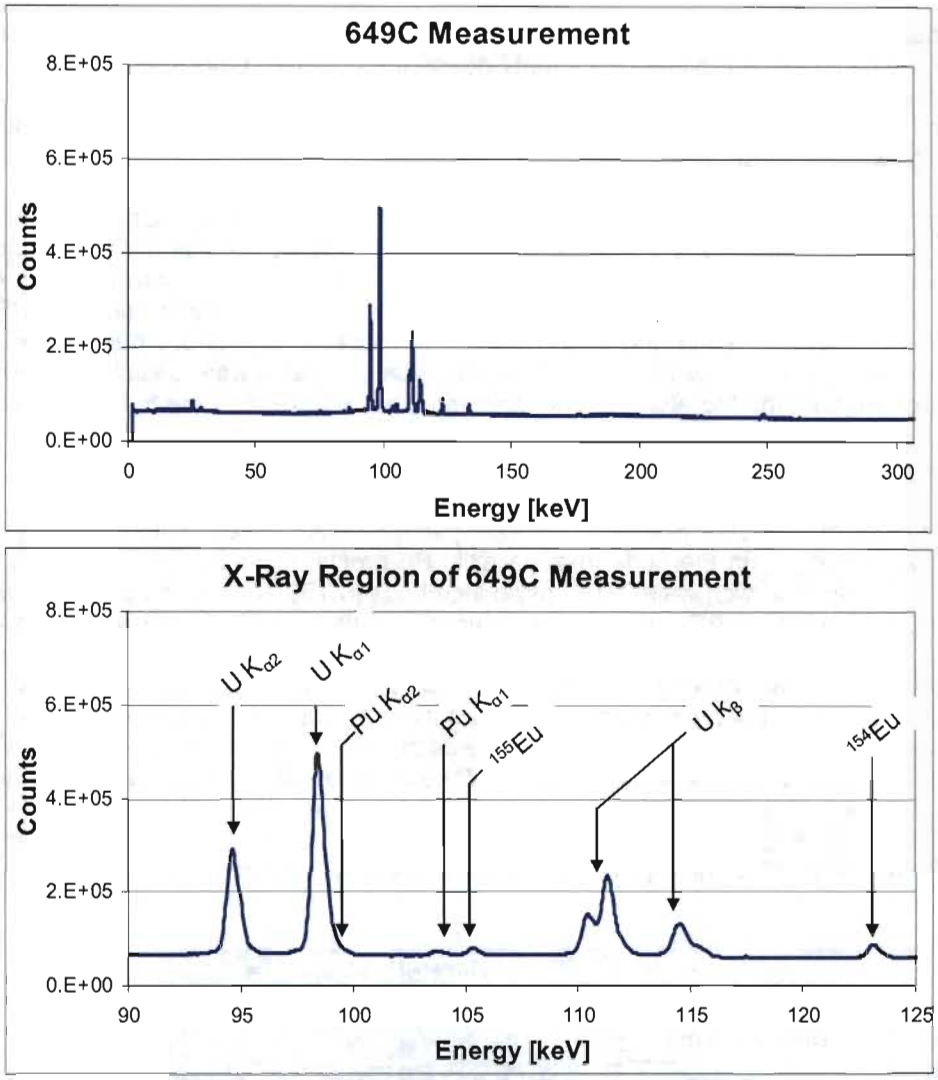

Figure 2: Measurement of pin 649C at ORNL with a planar HPGe detector. The live count was 44,263 seconds with 18% dead-time. Top: Full spectrum. Bottom: XRF region with peaks marked.

3.0 Simulating XRF Measurements of Fuel Pin 649C

The XRF measurements of North Anna spent fuel taken at ORNL presented an excellent benchmarking opportunity for the XRF models. MONTEBURNS/ORIGEN2 was used to calculate the isotopic inventories present in the fuel pin. The North Anna fuel pin had an initial enrichment of 4.2% and was burned to 67 Gwd/tU in three cycles with a final cool down of 4.7 years. The pellet radius was 0.40957 cm with a 0.00826 cm thick air gap and 0.05715 cm of cladding. Ten radial regions of decreasing thickness were used to capture the rapid increase of Pu concentration at the pin edge. Figure 3 shows the radial profile of Pu calculated for 649C.

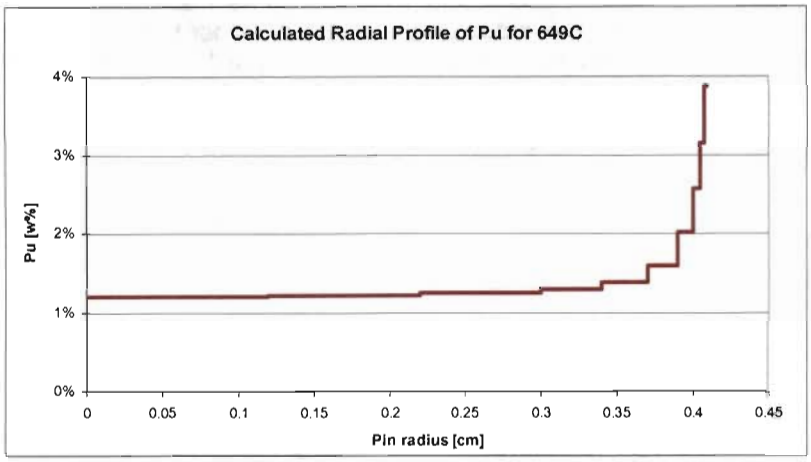

Figure 3: Radial profile of Pu calculated for pin 649C using MONTEBURNS/ORIGEN2.

3.1 Fluorescing Source Term

Only x-rays produced from beta and gamma excitation of the atom are considered in this work. The contribution of excitation from alpha particles and all other sources were considered negligible. Given that MCNPX modeling of electron transport for the determination of the XRF contribution from beta particles requires significant computational resources, research was done to see if simplifying assumptions could be made to minimize the amount of electron transport done. Therefore, simulations were done to determine the relative importance of the photon source and beta source in spent fuel as well as electron transport initiated by both of the aforementioned radiation sources.

The gamma source was calculated using a methodology and code that was developed for calculating delayed gamma source terms [7][8]. The code uses data libraries from CINDER'90 [9] for fission yields and reaction rates and uses Evaluated Nuclear Data Files (ENDF) for decay constants and branching ratios to produce a robust gamma source term from given isotopic inventories. Figure 4 shows the gamma source term created. Since the relative intensity of gammas spans many orders of magnitude, most of the gamma lines will be created too infrequently to be of consequence in the MCNPX calculation. The discrete gamma lines that failed to meet a relative probability of emission criteria were discarded in the source deck. The criteria was chosen based on the number of source particles sampled in MCNPX so that each photon source line that was kept was likely to be sampled at least a few hundred times throughout the run.

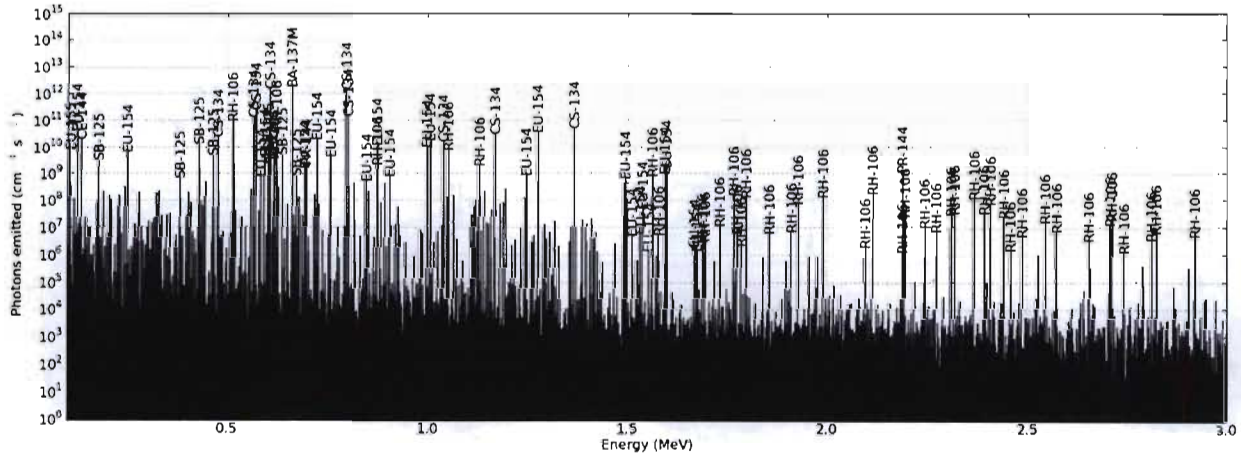

Figure 4: Gamma source term generated for gamma and beta comparison.

A literature search showed that comprehensive lists of beta emitters in spent fuel important to XRF are not well known. As a consequence, it is understood that while we think our beta source term has included the most important beta emitters that were tracked by the MONTEBURNS/ORIGEN2 code, it should be noted that this source term may be deficient. The intensity of beta particles emitted by each isotope in 1keV energy bins is available tabulated from Laurence Berkeley National Laboratory [10]. The combined binned energy spectrum for a single pin region is shown in Figure 5.

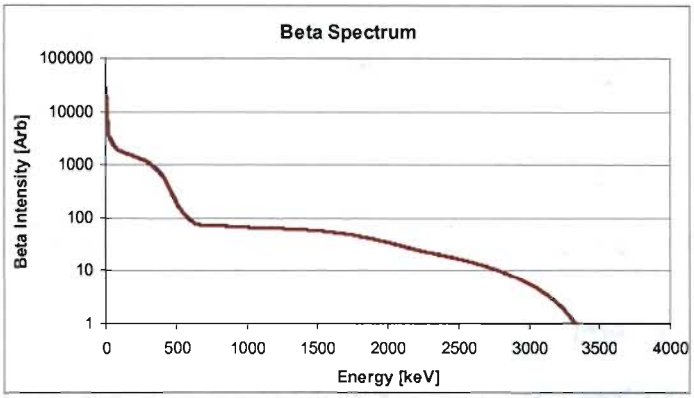

Figure 5: Calculated beta energy spectrum for a radial region in 649C.

A comparison of the x-ray signal strength induced by beta and gamma sources was performed to better understand the relative importance of both sources. For comparison, an MCNPX simulation was run of a 6 cm tall piece of fuel pin 649C. The photon signal exiting radially out of the stainless steel shipping tube was tallied in MCNPX for both source terms. Figure 6 shows the comparison between beta and gamma source terms in the XRF region. Calculations show that the majority of the contribution to the XRF signal is from the gamma source term. The beta source term was found to contribute roughly 10% to the XRF peaks. Since MCNPX transportation of beta induced XRF is orders of magnitude more computationally demanding than calculating its gamma counterpart, the remaining calculations will only involve the gamma term, with the understanding that a portion of the XRF signal is unaccounted for. The scenario simulated used the isotopic inventories calculated for fuel pin 649C. For our feasibility study, we have concluded that only simulating the gamma term will be sufficient to determine our key goal of relative Pu/U x-ray emission.

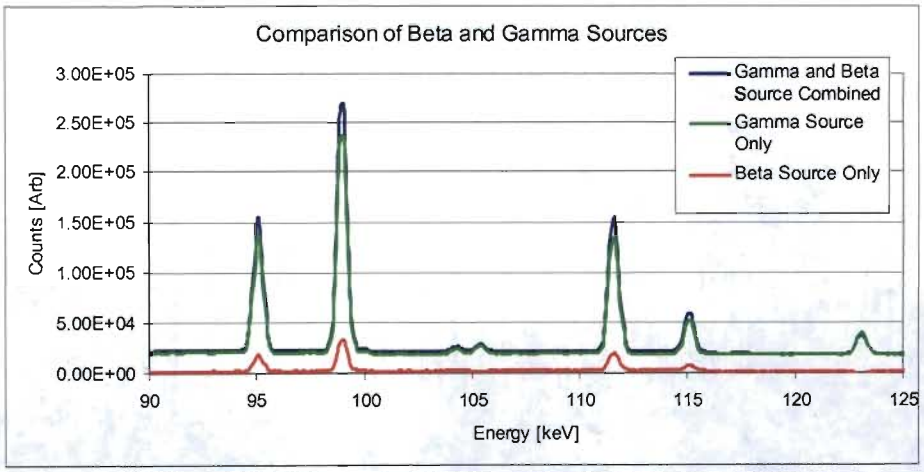

Figure 6: Comparison of beta induced and gamma induced XRF.

3.2 Radial Behavior of Source Term

An examination of what part of the fuel pin produces the measured U and Pu x-rays was conducted. Considering each of the ten regions modeled separately, the contribution to the U K_{a1} peak on a per source particle bases is plotted for gamma sources in Figure 7. Particles created closer to the outer radius of the fuel have a greater chance of contributing to the XRF signal. This seems intuitive as XRF signal that is created away from the outer edge is more likely to be attenuated. As the gamma source moves closer to the edge, however, the contribution to XRF begins to rapidly drop off. We interpret this as the gamma source at this point becomes more likely to escape itself than to create an x-ray to begin with.

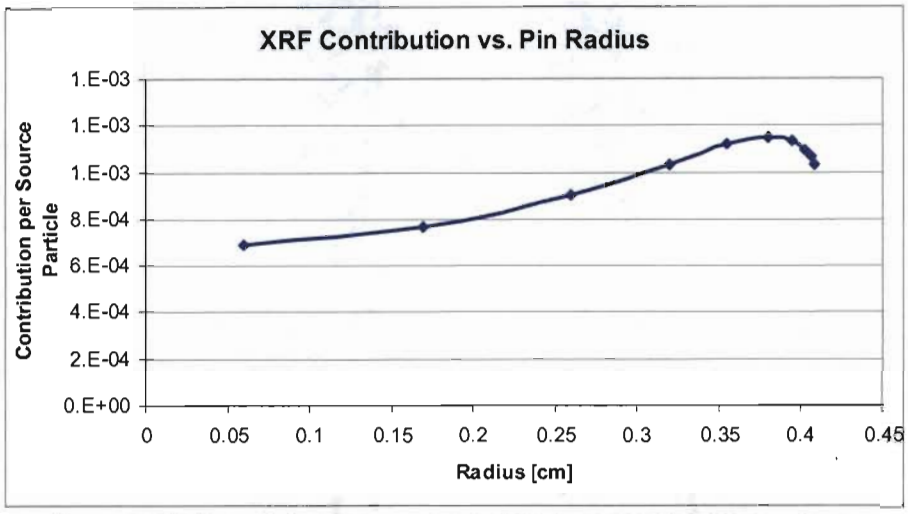

Figure 7: XRF signal that escapes the fuel pin by region for gamma source.

3.3 Modeling Methodology

To calculate the detector response in the HPGe crystal, the MCNPX f8 tally energy deposition is used. F8 tallies allow very limited variance reduction in MCNPX. Given that analog transport mode is required with f8 tallies, the number of particles that escape the fuel pin, travel down the long collimator, and interact in the detection crystal are too few and computationally inefficient for our resources. Therefore, we needed to make some simplifying assumptions. We decided to break the calculation into two pieces in order to bring the run-time down to a manageable range.

The first MCNPX model is a 6 cm tall fuel pin, including cladding and shipping tube, simulating 649C, to simulate the creation of x-rays inside the fuel. Only 6 cm of fuel pin is modeled because it was found that for a horizontal collimator with a radius of 0.1cm that is 5cm long centered on a 6 cm fuel pin, the probability of photons making it to the end of the collimator becomes negligible for sources in the fuel born about 2 cm above the center of the collimator. Therefore, modeling a longer fuel pin piece would not contribute to the MCNPX tally and would only require longer run times. The energy spectrum of photons exiting the shipping tube surface is tallied to approximate the energy distribution that is incident on the detector. Furthermore, collimator itself is modeled and the total number of photons that reach the end of the collimator is also tallied to approximate the fraction of photons that are incident on the detector per source gamma. The collimator is long enough that it is considered ideal, and thus, only the pin hole is modeled. This also significantly reduces the computational needs by not tracking multiple particle collisions and absorption in the collimator. Since the fuel pin is symmetric, the model is designed with multiple collimators like the spokes on a wheel to further increase the computational efficiency. The resulting total magnitude of every collimator is normalized by dividing by the number of collimators used. Figure 8 shows the MCNPX model with 180 collimators. Figure 9 shows a detailed look at the fuel pin modeled.

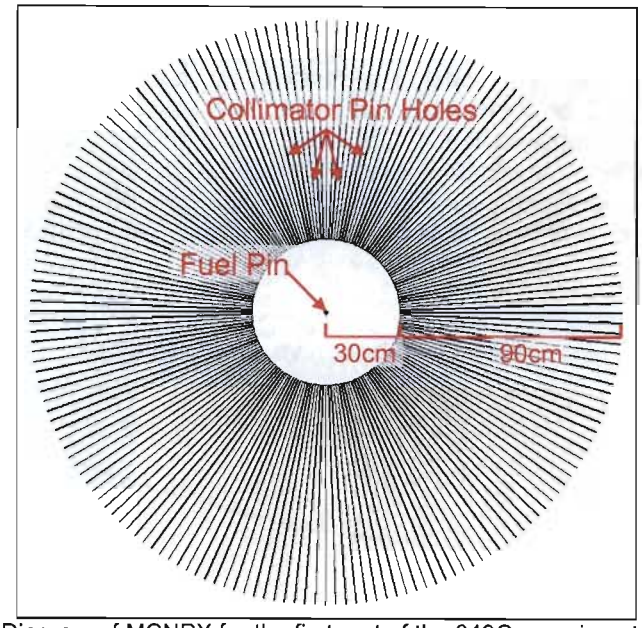

Figure 8: Diagram of MCNPX for the first part of the 649C experiment simulation.

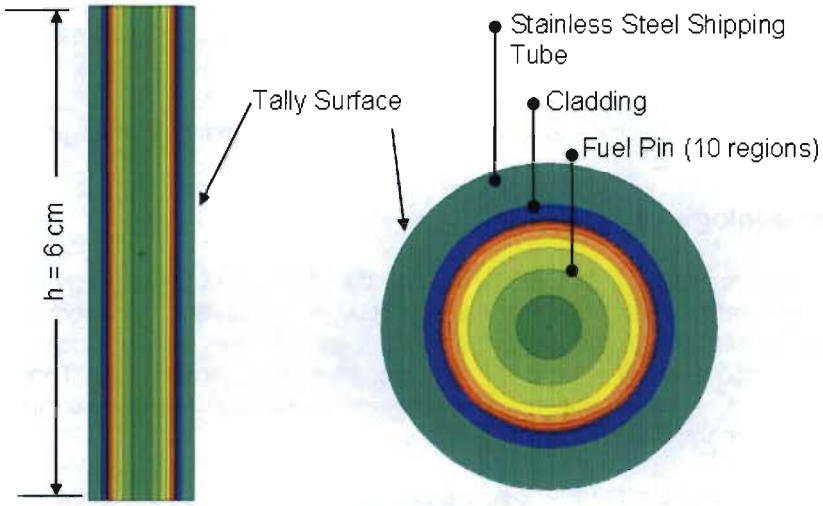

Figure 9: MCNPX geometry of the fuel pin.

Not all photons that exit the shipping tube were included in the MCNPX tally for energy spectrum. Photons created in the same location that exit the fuel pin with different angles to the surface normal cross different distances of material, and therefore are attenuated differently. Thus, tallying all photons that escape the fuel pin would unacceptably bias the tallied energy spectrum. The maximum angle that an ideal collimator, which is 90 cm long with a radius of 0.1 cm, allows is 0.127°. Tallying only photons that cross the surface normal near this angle is not computationally feasible. It was found that tallying only photons exiting the shipping tube within 20° of the surface normal offered sufficient tally statistics with a minimal bias to the energy spectrum. Therefore, the tallies used to approximate the energy spectrum exiting the shipping tube included photons with angles up to 20° to the surface normal.

The second part uses an MCNPX model focused on the detector response by tallying the spectrum of energy deposition in the HPGe crystal. The photon source particles are created perpendicular to the HPGe crystal with the energy distribution calculated in the first part. All uncertainties and angular information in the first simulation is lost. Since the detector face is much larger than the collimator pin

hole, the angular distribution of particles that make it to the end of the collimator is unnecessary. Furthermore, since the collimator is considered ideal, the Compton background from any photons that would have scattered off the collimator, but still contributed to detector counts are not included. The aluminum casing around the crystal, liquid nitrogen Dewar, cold finger, and the crystal structural casing inside the detector are included in the MCNPX model (Figure 10) for Compton background in the simulated detector. The HPGe crystal is 1.5 cm thick and 2.52 cm in diameter and is centered over the collimator hole. The MCNPX model includes a Gaussian Energy Broadening (GEB) card to account for the energy broadening properties of the HPGe detector. The final modeled spectrum is calculated by taking the simulated detector response from part two and normalizing it by the calculated total gamma source strength during the measurement live time multiplied by the fraction of source particles that reach the end of the collimator tallied in part 1.

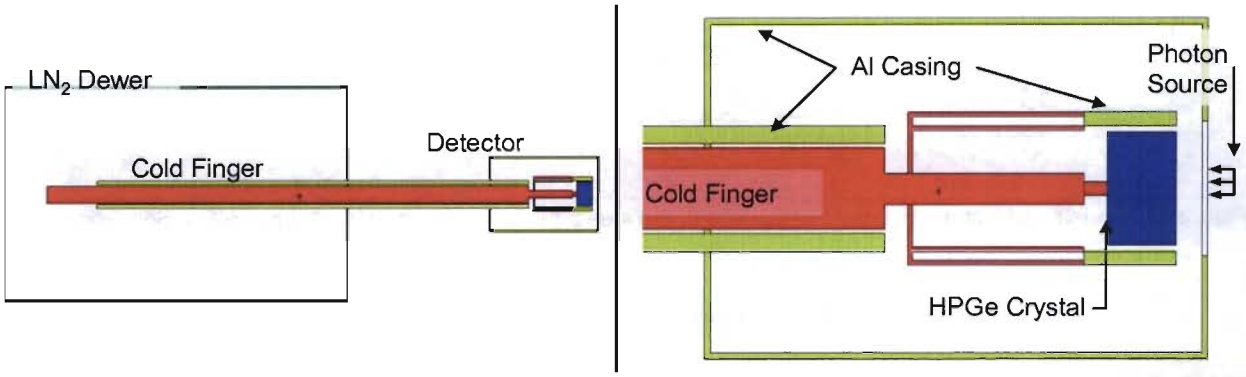

Figure 10: MCNPX for calculating the detector response. The photon tally from the first calculation is transported to the end of the collimator and used as the source. Left: Full geometry. Right: Close up of detector area.

3.4 649C Simulation Results and Comparison

In Figure 11 shows the results for the measurement and corresponding simulation are compared. Immediately it is noticeable that the simulated spectrum is lower in magnitude than the experiment; roughly by a factor of 30. Figure 12 shows the comparison focused on the x-ray region with the simulation results on a separate scale. There are several potential reasons for the discrepancy in magnitude. First, the beta term was ignored; however, the beta term alone cannot be the cause of the discrepancy because in both the simulation and measurement the Pu $K_{\alpha 1}$ x-ray and the ^{155}Eu gamma peaks (~105 keV) are roughly equivalent in magnitude. Given that both gamma and beta sources contribute to the x-ray peaks but only the gamma source contributes to the ^{155}Eu peak, if the ignored beta source term is in fact the dominant contributor, than the ratio of these two peaks would not agree between the simulation and experiment. Second, the ideal collimator assumption used to reduce run times causes lost photon counts. However, if ignoring the reflections inside the collimator was the problem then only the Compton background would be different, the measured and simulated x-ray peak heights would be similar. More probable explanations are that the normalization factor may be inappropriate for the methodology used of breaking the problem into two parts and/or the description of the experimental setup used to create the MCNPX models may be misunderstood, or flawed. For example, the collimator pin hole radius could be mistaken. Small increases in the collimator radius create large increases in the magnitude of the detector response.

A second thing to notice is the large background increase in the 200 keV area, which is significantly more pronounced in the simulation than in the measurement. This is a result of the back scattering off of the cold finger and other metal casings near the detector crystal. The modeled cold finger is based on visual inspection of other HPGe detectors, and has too much heavy material too near to the detector crystal. Fortunately, this effect has a minimal impact on the XRF region.

The comparison of the x-ray region in Figure 12 shows that MCNPX creates x-rays about 0.5 keV higher than seen in the measurement and given in Table 1. This discrepancy is a result of the data libraries used by MCNPX, which have incorrect values for the x-ray peaks tabulated in them. Furthermore, MCNPX incorrectly handles the K_β peaks. All K-shell to M-shell transitions are grouped together and emitted at a single energy, and all K-shell to N-shell transitions are likewise grouped together such that they are all created at the same energy.

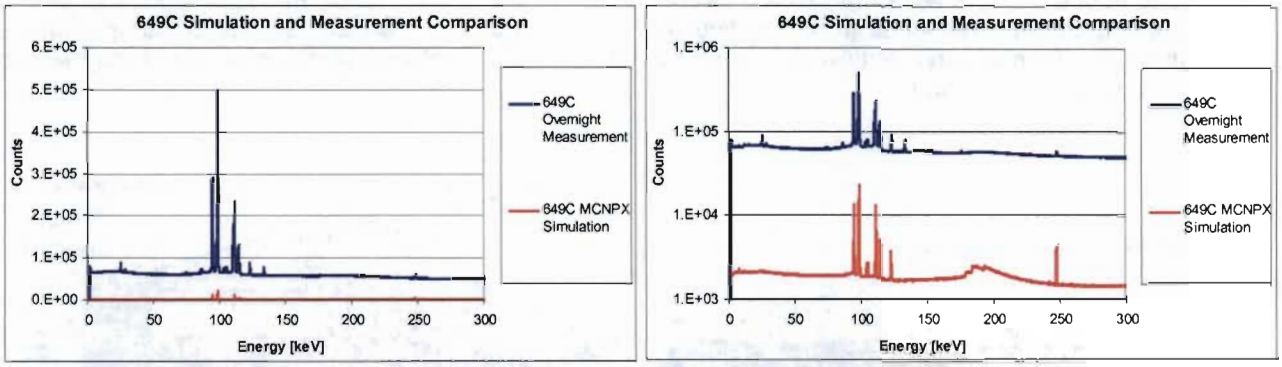

Figure 11: Modeled detector response comparison of the measurement and simulation for pin 649C. Semi-log scale.

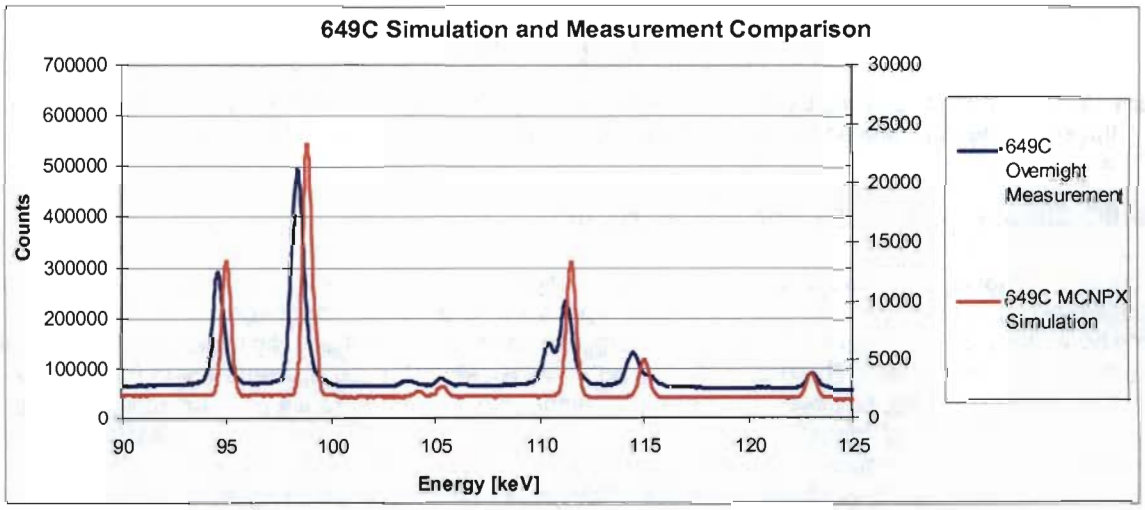

Figure 12: XRF region comparison of measurement and simulation for pin 649C.

3.5 Pu/U Ratio Comparison

The main goal of this work is to test the feasibility of using XRF signals in spent fuel assemblies to quantify elemental Pu through the ratio of Pu/U x-rays. As such, despite the scaling issue stated above, ultimately, the ratio of Pu/U that was simulated is the greatest importance.

To compare the Pu/U ratio between the measured and simulated spectrums, the net peak area of the U $K_{\alpha 1}$ and Pu $K_{\alpha 1}$ x-rays needed to be computed. This was done by averaging several bins on each side of the peak and connecting them linearly to estimate the background under the peak. Then the net peak was calculated by subtracting the estimated background from the total peak counts. Figure 13 and Figure 14 show the U and Pu peaks for both the simulation and measured data. In each case, the different areas marking where the continuum background was averaged along with the estimated peak background is illustrated. The uncertainty for each bin uses counting statistics, where $\sigma_{N,i}$, the uncertainty for bin i, is the square root of the number of counts, N_i. No uncertainties for the MCNPX calculation are carried over, and

no uncertainties in the isotopic inventories or source creation are considered. The measured U $K_{\alpha 1}$ and Pu $K_{\alpha 2}$ x-rays are not resolved, such that the Pu $K_{\alpha 2}$ x-ray becomes the tail to the U $K_{\alpha 1}$. From Table 1, the relative intensity of the Pu $K_{\alpha 2}$ x-ray is 62.5% of Pu $K_{\alpha 1}$. Therefore, the expected counts for Pu $K_{\alpha 2}$ can be estimated by multiplying the net counts for Pu $K_{\alpha 1}$ by 0.625. The net counts that should be attributed to just the U $K_{\alpha 1}$ peak are approximated by subtracting out the estimated counts for Pu $K_{\alpha 2}$. For the simulation, the two peaks are resolved enough so that the overlapping was considered negligible.

As discussed earlier, MCNPX produces the U and Pu $K_{\alpha 1}$ x-ray at the incorrect energy. This energy shift becomes a problem when calculating the net counts for Pu because the peak has significant overlap with the ^{155}Eu gamma peak. To avoid this problem, the Pu peak produced by MCNPX in part 1 was shifted down to the correct energy before using the spectrum as the source for part 2. This correction allowed the detected Pu x-ray peaks to be significantly resolved from the ^{155}Eu gamma line such that the overlap is ignored.

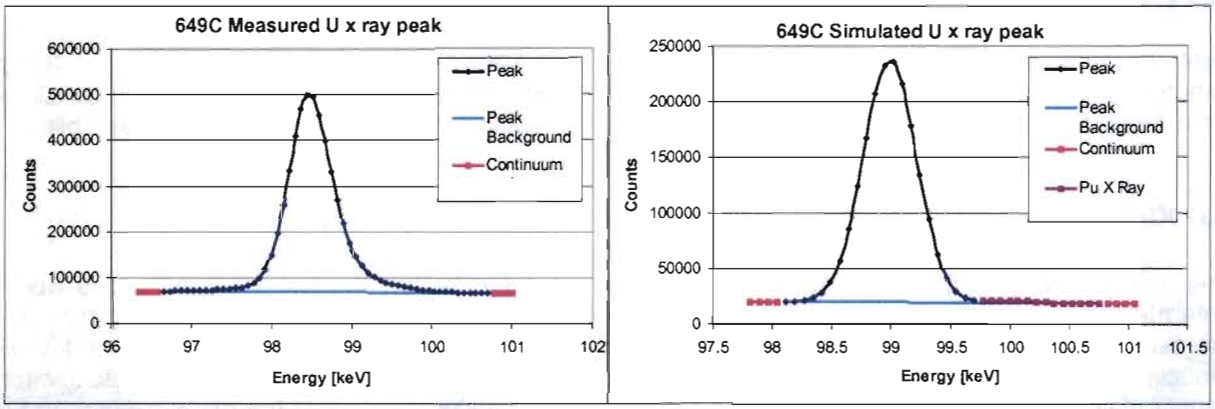

Figure 13: U $K_{\alpha 1}$ peak for 649C. Left: Measured. The tail on the right hand side includes the Pu $K_{\alpha 2}$ peak. Right: Simulated.

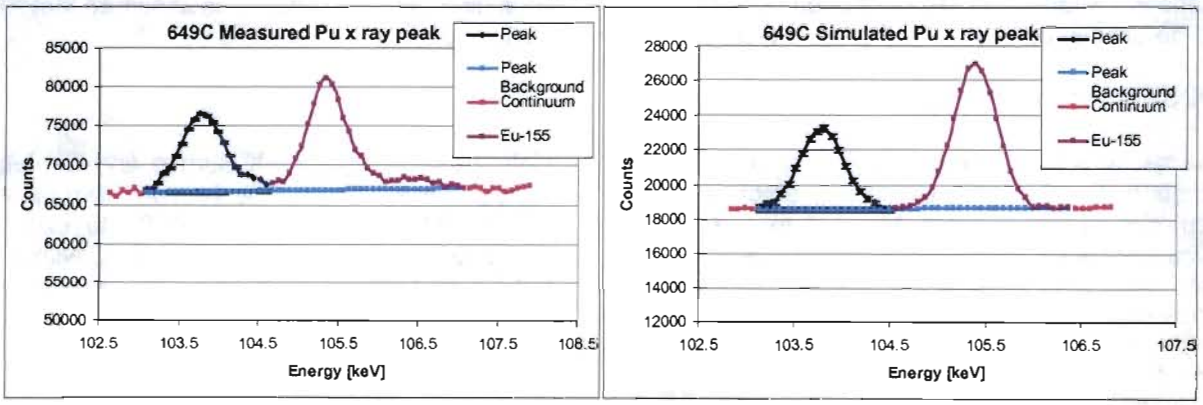

Figure 14: Pu $K_{\alpha 1}$ x-ray for 649C. Left: Measured. Right: Simulated. The energy of the Pu x-ray in the simulation case was corrected in the source term of the MCNPX detector response calculation.

Table 2 gives the results of the peak comparison for pin 649C. The uncertainties are the propagation of counting statistics from each bin. The simulation does an excellent job of calculating the Pu/U ratio, giving the ratio 0.0221±0.0004 compared to the measured ratio of 0.0227±0.0008. The simulated Pu/U ratio differs from the measurement by 2.7%, which is within two sigma of the measured value.

		Total			Peak Background			Net			
U	Measured	7,963,677	+/-	2,822	3,797,929	+/-	1,949	4,107,395	+/-	3,603	(0.1%)
	Simulated	845,405	+/-	919	176,331	+/-	1,956	669,074	+/-	1,011	(0.2%)
Pu	Measured	1,492,617	+/-	1,222	1,399,252	+/-	5,156	93,365	+/-	1,701	(1.8%)
	Simulated	159,962	+/-	400	145,156	+/-	381	14,806	+/-	552	(3.7%)
Pu/U	Measured	0.0227	+/-	0.0004 (1.8%)							
	Simulated	0.0221	+/-	0.0008 (3.7%)							

Table 2: Comparison of Pu and U x-ray peaks for 649C.

There are still many sources of uncertainty that are not accounted for in the above analysis. For example, the inventories calculated for the fuel pin will not be exact. The MCNPX uncertainties for both calculation parts were ignored, and the model itself creates bias because it is a simplification of the measurement setup. Furthermore, the MONTEBURNS/ORIGEN2 depletion code used to calculate the inventories in the model has error that is ignored as well. Destructive analysis is planned for the 649 rod cuts at ORNL in the future; at that point the accuracy of the isotopic inventories can be examined.

Even though the magnitude of the 649C spectrum simulation is wrong, more important is that the 649C pin benchmark does provide confidence that the Pu/U ratio can be predicted. This is an important conclusion since it provides confidence in our ability to make predictions about XRF measurements of assemblies.

4.0 XRF Assembly Models

The suite of MCNPX spent fuel assembly models created for the NGSI effort are used in this work to determine the general behavior of XRF as a function of BU, initial ^{235}U enrichment (IE), cooling time (CT), the overall feasibility, and general limits of detectability for XRF in the context of full assemblies. MCNPX modeling is used to simulate the XRF signal that would be measured with planar HPGe detector for a variety of light-water reactor (LWR) assemblies measured in water. Given that the mean free path of the XRF signal in nuclear fuel is ~0.5mm, obviously this measurement technique is completely blind to scenarios where fuel pins have been removed (that are not in direct field of view). It is assumed that XRF will be used in combination with other techniques more sensitive to fuel pin diversions.

4.1 Spent Fuel Library

The set of spent fuels assemblies created for the NGSI effort used the MCNPX Burnup and Depletion capability to create the isotopic inventories of pins throughout the assembly. The MCNPX Burnup and Depletion capability uses MCNPX to calculate neutron fluxes at power and CINDER'90 to explicitly calculate the subsequent buildup and decay of isotopic inventories for each time step. While CINDER'90 uses a data set of 3400 nuclides, MCNPX discards all but the few hundred isotopes that have neutron cross sections available for calculating flux. It is assumed that the isotopes tracked are significant for our purposes. The array of assemblies produced is referred to as the spent fuel library (SFL) and consists of the 64 combinations of the following: 15, 30, 45, and 60 Gwd/tU BU; 2, 3, 4, and 5% IE; and 1, 5, 20, and 80 years CT.

Memory allocation limitations with the MCNPX code used to produce the SFL confines the number of BU materials to a few hundred. Restricting the number of radial regions down to four for each pin, results in a loss of fidelity in modeling the radial Pu. Furthermore, only one vertical region was modeled, thus, there is no vertical BU profile in the SFL used in this work.

The assemblies created for the SFL used a 17 by 17 Westinghouse LWR assembly with infinitely reflected boundaries. This boundary condition is good for creating generic assemblies; however, it neglects asymmetries in BU throughout the core that arise from fuel loading schemes. Asymmetries in BU, and therefore Pu, may be particularly difficult for the XRF technique to handle because the measured U and Pu x-rays can only be sampled from the front row of pins. Extrapolating the Pu content of the whole assembly from the measured outer pins will be complicated by these asymmetries.

Recent improvements in the MCNPX code have alleviated memory restrictions to some degree, increasing the potential number of materials that can be burned [11]. Combined with increases in computational resources, the MCNPX code improvements have allowed a current effort to create a new SFL. This second SFL is being created with a $1/8^{th}$ core model so that neighboring assemblies can be on different cycles. Assemblies created in this new SFL will have a better representation of asymmetries in BU resulting from reactor loading schemes [12]. Exploring the effect of BU asymmetry in the assembly is a topic for future work in XRF.

4.2 Modeling Methodology

The methodology for simulating detector response to spent fuel assemblies is similar to the methodology employed for simulating pin 649C in that the MCNPX component is broken down into two parts. The first step is to calculate the initial source, then use MCNPX to calculate the photon spectrum that escapes one face of the assembly. Next, the magnitude is corrected for geometry of the collimator, and finally, another MCNPX simulation is used to calculate the detector response, using the energy spectrum from the first MCNPX calculation as the source for the second. Figure 15 illustrates the methodology.

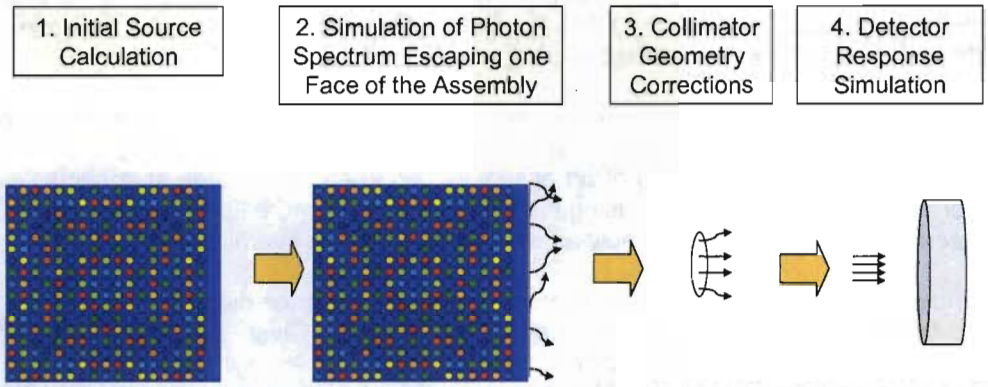

Figure 15: Graphical representation of the methodology used for calculating the XRF response for an entire assembly.

Using the isotopic inventories created for the SFL described above, the same code used to calculate the gamma source for the 649C benchmark is used to create the gamma source definition for the entire spent fuel assembly. Only the gamma source is considered. In the 649C pin simulations, the beta source was estimated to contribute 10% to the XRF signal.

There is also reason to believe beta particles will be less important for assembly measurements than single pins. High energy photons in inner pins can penetrate to the outer pins where fluorescence of U and Pu can contribute to the x ray signal. Betas born in inner pins deposit their energy locally and only some fraction will produce a high energy gamma as a secondary particle to transport their energy through the assembly to the edge.

The assemblies are 21.42 cm to a side and only 6 cm of rod height is modeled. There is a possibility that structural objects or operator regulations may prevent a collimator from being placed directly against the side of the assembly. Therefore, 1.5 cm of water is modeled on the side of the assembly that is tallied. In MCNPX, a surface tally with energy bins of 0.1 keV is used to calculate the spectrum that escapes the side of the assembly being measured. Since the SFL has symmetrical BU on each side, there is no difference on which side is tallied. Similar to the simulation of 649C, a maximum angle of 20° to the surface normal is allowed in the tally. Figure 16 shows the MCNPX model used for comparing the Pu/U ratios of the SFL.

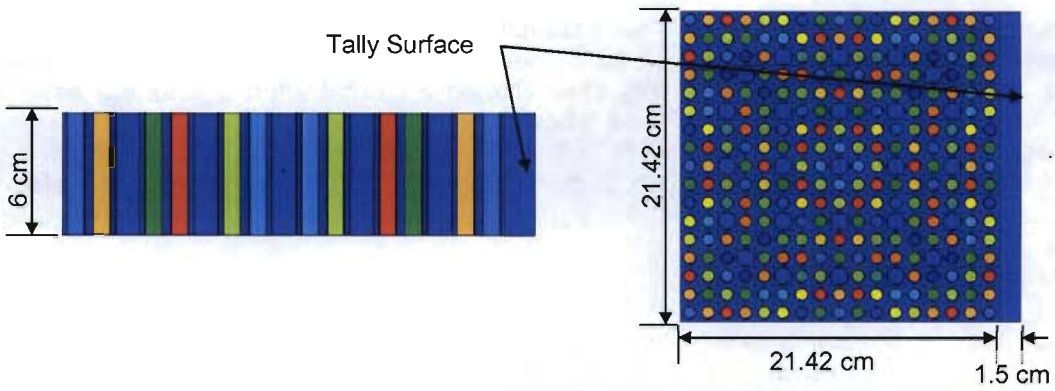

Figure 16: MCNPX model of spent fuel assembly. One side has 1.5 cm of water and is tallied on.

It is important to note that with this modeling setup, one whole side of the assembly is tallied together. Therefore, spatial information from a single pin or section is effectively lost. Our current computational resources force the use of this technique. However, given that the desired quantity is Pu in an assembly, measuring multiple pins will be necessary in any event. Thus, taking the tally of an entire side will be relatable to the measurement sum of each pin along one face of the assembly.

A collimator that receives photons from an entire assembly side will likely have too high of a count rate or too narrow a slit to be practical given the need to keep the count rate low. Using a pinhole collimator is more realistic. Scanning across the side of an assembly can keep count rates at acceptable levels while measuring more than one pin. However, using multiple detectors is more likely as a means of determining the Pu mass across the face of the assembly as well as reducing the overall count time.

Unlike the simulations of 649C, there is no pre set collimator length or diameter. Therefore, one can be chosen that optimizes the count rate experienced by the detector. Given that the source strength of the assemblies tested varies drastically - consider 1 and 80 years CT - it will be beneficial to have several different collimator sizes. The magnitude of the detector response tallied in the second MCNPX calculation will need to be normalized to the gamma source strength of the assembly and the collimator used. Unlike the 649C benchmark, the correction for the collimator will be calculated by considering two basic components of the MCNPX tally and the collimator. The benefit of calculating correction factors for the collimator over using MCNPX as in the 649C benchmark is that count rates in the detector can be adjusted in post processing, instead of requiring multiple MCNPX runs for different collimator dimensions. The first step is a correction factor for the difference in area that is tallied, A_{TALLY}, and the cross sectional area of the collimator, A_{TRUE}. This correction factor, f_{Area}, is calculated with the equation below.

$$f_{AREA} = \frac{A_{TRUE}}{A_{TALLY}}$$

The second correction factor takes into account the fact that the MCNPX tallies all photons that escape the tally surface at an angle below 20° to the surface normal. The angular correction factor, f_θ, is calculated by taking the ratio of steradians, Ω, between the maximum angle that incident photons can reach the end of the collimator with, θ_{TRUE}, and the maximum angled tallied, θ_{TALLY}, collimator and what was tallied.

$$f_\theta = \frac{\Omega_{TRUE}}{\Omega_{TALLY}} = \frac{1-\cos\theta_{TRUE}}{1-\cos\theta_{TALLY}}$$

The normalization constant applied to the MCNPX detector response spectrum is the product of the total source strength of gammas over the measurement time, f_{Area}, and f_θ. This approach implies an ideal

collimator, as well as a collimator hole under vacuum. For measurement purposes the collimator hole will need to be sealed from water to avoid complete attenuation of the x ray signal.

Tolerable count rates of $3 \cdot 10^4$ to $5 \cdot 10^4$ Hz can be expected from commercial equipment (although 10^5 Hz is available as well). In this work, the modeled collimator dimensions are chosen so that the total count rate experienced by the detector - including events that are rejected by the lower level discriminator and events that are above the gain settings - stay in that range. Since the magnitude of the 649C benchmarking was off by an order of magnitude and the normalization uses a different method, there is no reason to expect the assembly modeling not also be off in magnitude. This is of little consequence since the magnitude of the detector response can be adjusted in measurements by adjustment in collimator aperture and the large variation of source intensities will already require a set of different sized collimators. More importantly, regardless of how different the collimator modeled and the actual collimator end up being, as long as the count rate experienced by the actual detector falls into the range used as the criterion for choosing the modeled collimator, then the live-times and counting statistics presented in the following work will still be accurate.

4.3 Signal Contribution by Assembly Row

One of the limiting factors in application of XRF is the lack of penetrability of a 100 keV photon through fuel. The mean free path of x-ray energy photons in nuclear fuel is about 0.05 cm. Thus, x-rays created in the second row of pins have a negligible chance of crossing through a front row pin to reach a collimator or detector. This problem is compounded by the high count rate which limits collimation to one pin and potentially by the high energy photons emitted by fission products deeper in the spent fuel assembly, which can penetrate through several rows of fuel. Therefore, pins not in the front row can contribute to Compton background with high energy gammas, but their x-rays never make it to the detector.

Using an assembly with 60 GWd/tU BU, 4% IE, and 5 year CT, the detector response to each row in the assembly is simulated. A collimator 80 cm long with a radius of 0.15 cm and a live-time of 3600 seconds is assumed. The total count rate calculated on the detector is about $4.6 \cdot 10^4$ Hz. Figure 17 shows the contribution to the signal from each row for the U $K_{\alpha 1}$ energy region and Figure 18 plots the percentage of net peak and background for each row. Both the x-ray signal and background contributions drop off very rapidly in the first five rows. By the ninth row, the contribution to net peak signal is down to 0.1%, and the background is 0.6%. Effectively, the second half of the assembly does not significantly contribute to the signal or background. Rows 9 through 17 combine to contribute less than 0.5% to the net peak and 2% to the background. An important point to note is that the rows beyond the first row do contribute to XRF signal. X-rays created outside of the first row don't contribute to the signal, but the higher energy gamma field that penetrates to the first row does create x-rays in the first row that do contribute to signal. This allows the x-ray signal to grow almost proportionately with the Compton background, which means that the additional rows of pins in an assembly won't necessarily mask the Pu x-ray signal.

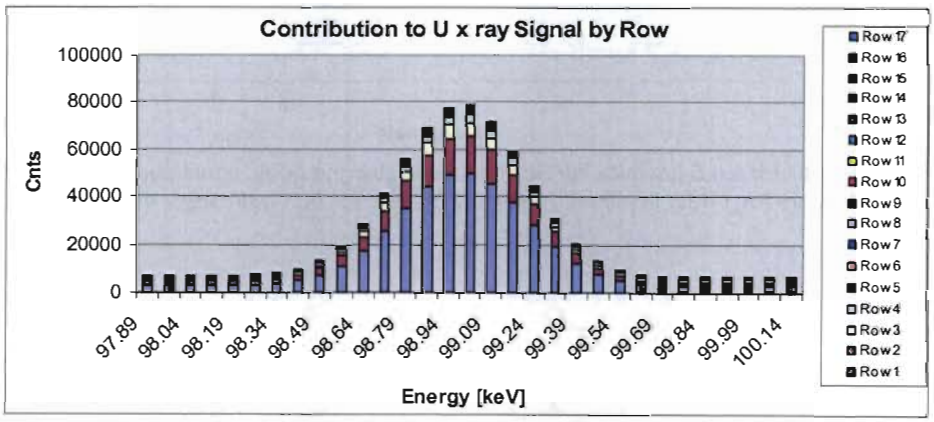

Figure 17: Contribution of each row to the total peak measured. 60 Gwd/tU BU, 4% IE, and 5 year CT, with a 3600 s live-time.

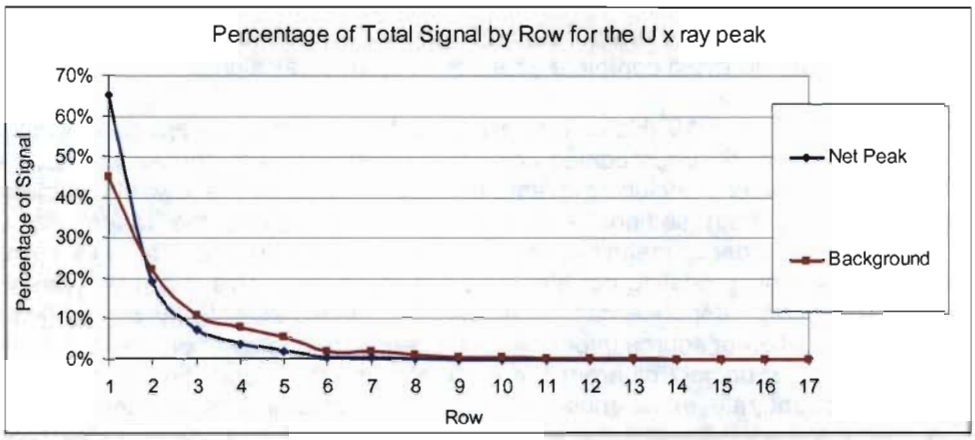

Figure 18: The contribution of each row to the detected signal and background for the U $K_{\alpha 1}$ peak.

4.4 Detector Crystal Thickness

To minimize count time, it is desirable to choose a detector crystal that provides the highest signal-to-background for the x-ray peaks of interest. For detector optimization, the 45 Gwd/tU BU, 4% IE, and 5 year CT assembly was used. MCNPX simulations using the model seen in Figure 10, except with varying crystal thicknesses, were run. Thickness ranged from 1.5 cm, like the crystal used in 649C, down to 0.1 cm. A collimator 80 cm long with a diameter of 0.15 cm is assumed. The count rate experienced by the different detectors ranged from 3.2 to $4.4 \cdot 10^4$ Hz. Figure 19 shows the peak with uncertainties for counting statistics assuming a 1 hour count time, and Figure 20 shows the calculated signal to background ratio for the Pu x-ray peak as a function of detector thickness. The Pu $K_{\alpha 1}$ x-ray is the peak examined for comparison because its smaller signal makes it the limiting factor in measuring the Pu/U ratio accurately. A detector crystal with a thickness between 0.25 cm and 0.75 cm should be optimal for measuring XRF of spent fuel assemblies. In the remaining work, the HPGe crystal thickness used is 0.5 cm.

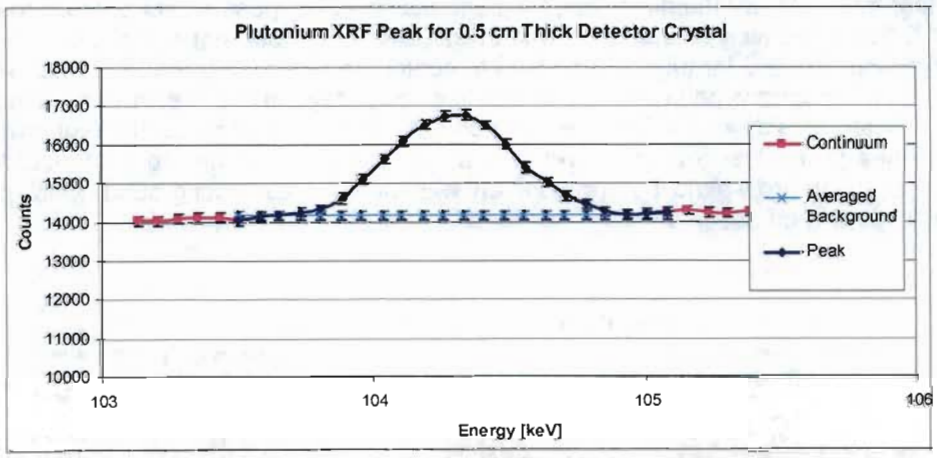

Figure 19: Pu x-ray peak for a 0.5 cm thick HPGe crystal showing the peak, continuum, and peak background. Counting statistics are for 1 hour live-time. Assembly modeled is 60 Gwd/tU BU, 4% IE, and 5 year CT.

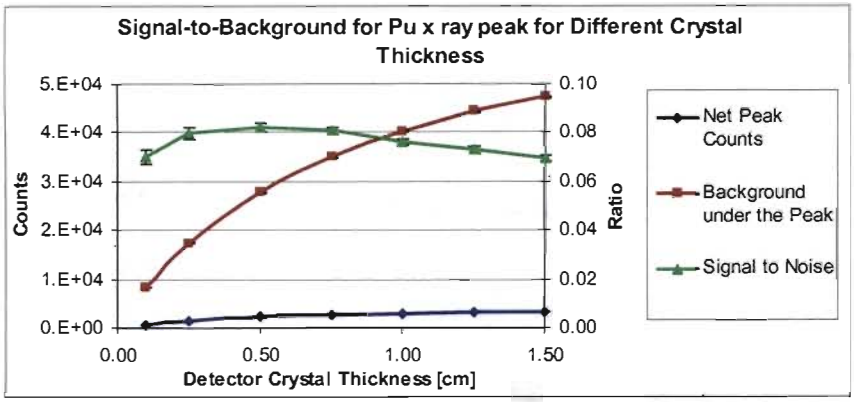

Figure 20: Signal-to-background ratio as a function of HPGe crystal thickness for the Pu x-ray peak. Counting statistics are for 1 hour live-time.

4.5 Detector Crystal Radius

This section examines the signal-to-background for x-rays of interest for various crystal radii. In the 649C measurements, a crystal radius of 1.26 cm was used. The collimator radius was only 0.1 cm. Therefore, much of the crystal was unused. Radii simulated ranged from 1.26 cm, like the crystal used in 649C, down to 0.25 cm. Figure 21 shows the calculated signal to background ratio for the Pu x-ray peak as a function of HPGe crystal radius. These simulations suggest that the effects of radius are not as important as crystal thickness. This is expected since the photon beam is directed at the entire thickness of the crystal, but the collimator forces the beam to be directed at only 0.15 cm of radius. Since the collimator radius for measuring assemblies is not set, a good choice of crystal radius may be at least twice the radius of the collimator. The remaining models use a 0.5 cm radius HPGe crystal.

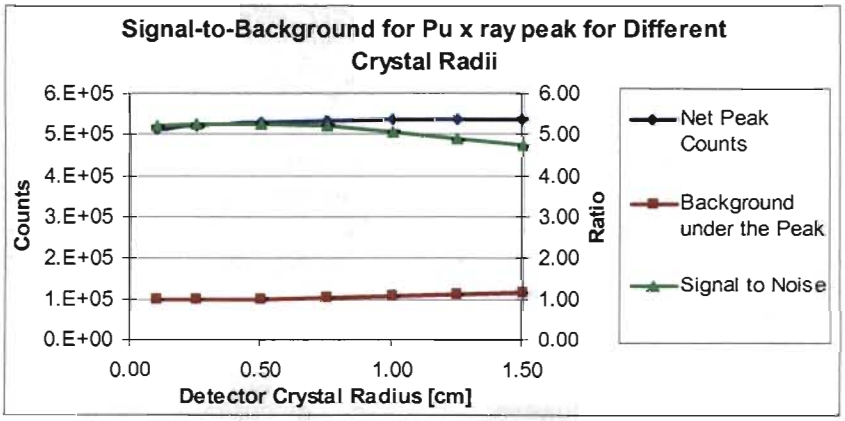

Figure 21: Signal-to-background ratio as a function of HPGe crystal radius for the Pu x-ray peak. Counting statistics are for 1 hour live-time.

4.6 Water Thickness

Different conditions among facilities make the amount of water that will be present between the assembly and collimator an unknown variable. The mean free path of 100 keV photons in water is approximately 6 cm; therefore, small amounts of additional water are not expected to impair XRF. Thicknesses of water were simulated ranging from 0 to 2 cm. Figure 22 shows the calculated signal-to-background ratio for the Pu x-ray peak as a function of water thickness. Having a collimator 2.0 cm away from the assembly is expected to drop the signal-to-background roughly 30% below the case where the collimator is touching

the assembly. The assembly cases discussed later comparing BU, IE, and CT, all assume that 1.5 cm of water is between the assembly and collimator.

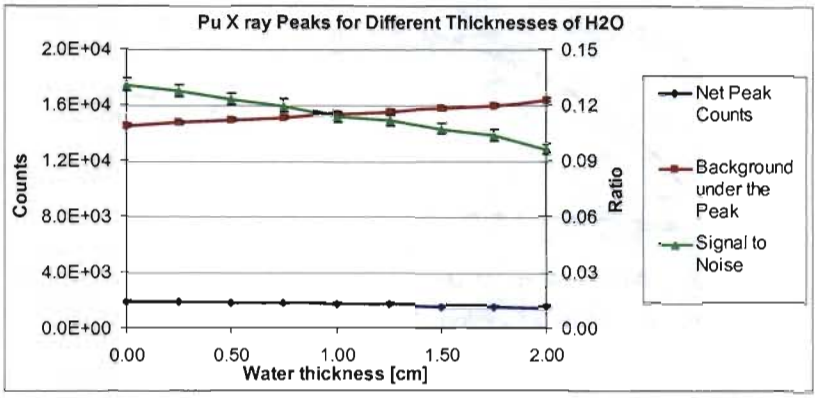

Figure 22: Signal-to-background ratio as a function of H_2O thickness between the assembly and collimator. Counting statistics are for 1 hour live-time.

4.7 Pu/U Ratio of Spent Fuel Assemblies

Using the methodology described above, the suite of SF assemblies in the SFL was simulated using an HPGe crystal that was 0.5 cm thick with a 0.5 cm radius. The collimator dimensions needed to be varied to adjust for the wide range of photon source strengths. For example, the photon source strength of assemblies with 80 year CT typically is ~20 times weaker than the 1 year CT scenario. Assuming that five collimators, 80 cm long with radii of 0.3, 0.25, 0.2, 0.15, and 0.1 cm, are available, for each assembly the biggest collimator was chosen such that the count rate experienced by the detector was less than $4 \cdot 10^4$ Hz. The Pu/U XRF ratios calculated compared to the Pu/U mass ratios for the SFL is plotted in Figure 23 grouped by BU (color) and IE (shape). CT has a small impact on the Pu/U ratio, the exception being 80 years CT, where the 14 year half-life of ^{241}Pu and 87.7 year half-life of ^{238}Pu can reduce the Pu mass significantly. CT does significantly affect the total source strength. As expected, BU has a large impact on Pu and thus, the Pu/U ratio. The 15 Gwd/tU BUs are grouped together with much lower Pu/U ratio than the rest.

The uncertainties in the inventory calculation as well as the MCNPX models are completely ignored in the results. Since the problem is broken into two parts, the uncertainties in the first part are lost by default. The uncertainties presented are from counting statistics for a 1 hour live-time, and are unrelated to all of the modeling uncertainties that were ignored. Hence, this is why none of the 64 data points in Figure 23 are outside 1 sigma from the linear relationship.

The linear fit for the data shows a very strong correlation with an R^2 value of 0.9899. This suggests that if counting statistics can be driven down by an appropriate collimator and count time, XRF may be used to accurately determine the Pu quantity. However, it has been demonstrated that the Pu/U XRF signal from the assembly is really a representation of the Pu/U mass ratio in the front row of pins. The reason it matches so well to the Pu/U mass ratio of the assembly is due to the material symmetry of the assembly caused by assuming infinite boundaries. Depletion calculations which use spent fuel assemblies with a more realistic fuel loading, and therefore asymmetries in the Pu distribution, need to be modeled to determine a more accurate representation of how the Pu/U XRF signal will compare to the Pu/U mass in an assembly.

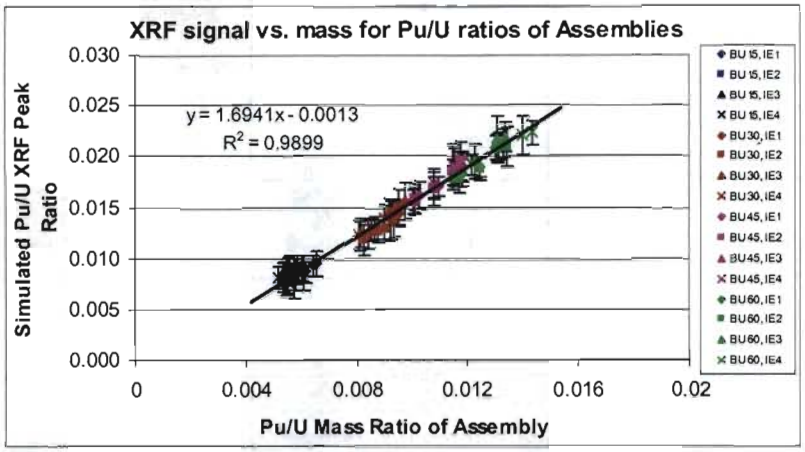

Figure 23: Simulated Pu/U x-ray ratio compared to the Pu/U mass ratio of the assembly. All modeling uncertainties are ignored. Uncertainties presented are from counting statistics assuming a 1 hour live-time using various sized collimators. Hence, none of the 64 data points appear outside 1 sigma from the linear relationship.

Table 3 lists the Pu/U mass ratio, Pu/U XRF simulation ratio for the 64 assemblies modeled, the collimator radius used, along with the XRF simulation uncertainty from counting statistics for a 1 hour and 10 hour measurement. For a 1 hour count time, the highest relative uncertainty for the XRF Pu/U ratio was 19.1%, which corresponds to an uncertainty on the Pu/U mass ratio of 15.5%. Excluding the low Pu/U ratios of the 15 Gwd/tU BU cases, the highest uncertainty on the XRF Pu/U ratio was 14.1%, corresponding to 12.5% uncertainty for the Pu/U mass ratio. For the 10 hour count time the highest uncertainty was 6.0% for the XRF Pu/U simulation, which corresponds to 3.6% uncertainty for the Pu/U ratio of the mass in the SF assembly. The correlation for uncertainty is found by using the correlation from the linear fit in Figure 23.

For reasonable results with a single detector and a well chosen collimator diameter, a count time of at least 10 hours should be expected. This will not be acceptable for a technique that needs to quickly assay hundreds of assemblies. One solution is to have an array of collimators and detectors collecting and combining signals from an assembly.

Burnup	Initial ^{235}U Enrichment	Cooling Time	Pu/U Ratio		Collimator Radius	Uncertanty From Counting Statistics	
			Mass From	XRF			
[GWd/MtU]	[%]	[Years]	SF Library	Measurement	[cm]	1 hour	10 hours
15	2	1	0.0065	0.0095	0.15	13.7%	4.3%
		5	0.0064	0.0093	0.2	11.2%	3.5%
		20	0.0061	0.0087	0.25	11.3%	3.6%
		80	0.0059	0.0088	0.3	15.4%	4.9%
	3	1	0.0061	0.0085	0.15	16.0%	5.1%
		5	0.0060	0.0090	0.2	11.8%	3.7%
		20	0.0058	0.0089	0.25	11.0%	3.5%
		80	0.0056	0.0088	0.3	15.5%	4.9%
	4	1	0.0058	0.0082	0.15	17.3%	5.5%
		5	0.0057	0.0081	0.2	13.4%	4.2%
		20	0.0055	0.0084	0.25	11.6%	3.7%
		80	0.0054	0.0085	0.3	16.1%	5.1%
	5	1	0.0055	0.0076	0.15	19.1%	6.0%
		5	0.0055	0.0081	0.2	13.5%	4.3%
		20	0.0053	0.0081	0.25	12.1%	3.8%
		80	0.0052	0.0081	0.3	16.9%	5.3%
30	2	1	0.0098	0.0156	0.1	11.0%	3.5%
		5	0.0095	0.0145	0.15	8.1%	2.6%
		20	0.0090	0.0130	0.2	8.4%	2.6%
		80	0.0084	0.0124	0.25	11.4%	3.6%
	3	1	0.0095	0.0150	0.1	12.0%	3.8%
		5	0.0093	0.0146	0.15	8.3%	2.6%
		20	0.0088	0.0127	0.2	8.6%	2.7%
		80	0.0082	0.0119	0.25	11.8%	3.7%
	4	1	0.0094	0.0140	0.1	13.4%	4.3%
		5	0.0092	0.0146	0.15	8.5%	2.7%
		20	0.0087	0.0131	0.2	8.4%	2.6%
		80	0.0082	0.0126	0.25	11.2%	3.5%
	5	1	0.0092	0.0137	0.1	14.1%	4.5%
		5	0.0090	0.0140	0.15	9.1%	2.9%
		20	0.0086	0.0129	0.2	8.5%	2.7%
		80	0.0081	0.0122	0.25	11.6%	3.7%
45	2	1	0.0118	0.0190	0.1	6.8%	2.2%
		5	0.0116	0.0184	0.1	11.3%	3.6%
		20	0.0109	0.0171	0.15	9.4%	3.0%
		80	0.0103	0.0162	0.25	7.2%	2.3%
	3	1	0.0118	0.0195	0.1	6.9%	2.2%
		5	0.0115	0.0185	0.1	11.5%	3.6%
		20	0.0108	0.0169	0.15	9.5%	3.0%
		80	0.0101	0.0158	0.25	7.4%	2.3%
	4	1	0.0118	0.0191	0.1	7.3%	2.3%
		5	0.0115	0.0189	0.1	11.5%	3.6%
		20	0.0108	0.0169	0.15	9.5%	3.0%
		80	0.0100	0.0156	0.25	7.5%	2.4%
	5	1	0.0118	0.0194	0.1	7.5%	2.4%
		5	0.0115	0.0190	0.1	11.7%	3.7%
		20	0.0108	0.0174	0.15	9.3%	2.9%
		80	0.0101	0.0158	0.25	7.4%	2.3%
60	2	1	0.0133	0.0213	0.1	5.2%	1.6%
		5	0.0130	0.0209	0.1	8.6%	2.7%
		20	0.0124	0.0189	0.15	7.5%	2.4%
		80	0.0118	0.0184	0.25	5.6%	1.8%
	3	1	0.0134	0.0209	0.1	5.3%	1.7%
		5	0.0131	0.0211	0.1	8.5%	2.7%
		20	0.0124	0.0188	0.15	7.5%	2.4%
		80	0.0117	0.0179	0.25	5.7%	1.8%
	4	1	0.0134	0.0219	0.1	5.3%	1.7%
		5	0.0131	0.0217	0.1	8.5%	2.7%
		20	0.0123	0.0195	0.15	7.3%	2.3%
		80	0.0115	0.0180	0.25	5.7%	1.8%
	5	1	0.0144	0.0223	0.1	5.3%	1.7%
		5	0.0140	0.0221	0.1	8.5%	2.7%
		20	0.0131	0.0208	0.15	6.8%	2.2%
		80	0.0121	0.0192	0.25	5.3%	1.7%

Table 3: List of Pu/U mass ratio, Pu/U XRF simulation ratio, collimator radius, and Pu/U uncertainty from counting statistics for both 1 hour and 10 hour count times for the suite of assemblies modeled.

The uncertainty in Table 3 for a single detector is determined by (1) the relative intensity of the peak to the continuum, which was modeled reasonably well in the 649C benchmark, and (2) the count rate limit of the detector system is adjusted to a near optimum value by increasing the collimator radius. Given the small spot size, this adjustment keeps the observed area limited to one pin. The conclusion can then be drawn that the uncertainty of a single detector cannot be improved above what is listed in Table 3. If the simulations for an assembly are off by an order of magnitude, as was the case for the pin result, one would simply reduce the collimator area by that factor and get the same uncertainty for a 1 hour count.

As a result, it can be concluded that a single detector XRF system would not be practical for a spot inspection systems at pool storage facilities since the uncertainty from count statistics after a 1 hour count would be between 7% and 12% (30 GWd/tU and 45 GWd/tU for 1 to 80 year cooling times). This count time is long for spot inspections and no correction has been made for extrapolating from a few to several mm^2 observation area on the edge to fuel to the total Pu in the assembly. A point for future research is how many detector crystals could be combined in a given volume, weight, cost system to make a practical system for spot inspection, depending on if it is shown to be feasible to extrapolate from the Pu determined on the edge of the assembly to the whole assembly. More specifically, it would be desirable to have a system that obtains uncertainty of ~2% in 1000s. Based on the results in Table 3, a reasonable estimate is that ~100 detectors will needed.

The next step is to think how an XRF system comprised of an array of detectors could meet the two other safeguard needs we are focused on. It is expected that an XRF system could be retrofitted into a reprocessing facility, and it certainly could be designed into any future reprocessing facility. If it is shown to be feasible to extrapolate from the Pu determined on the edge of the assembly to the whole assembly, then a point of necessary future research is to determine how many detectors can be practically positioned around the assembly. It is anticipated that, with enough funding, the uncertainty could be reduced to below 2%. Furthermore, an array of detectors around the assembly would be a necessary step in doing the best possible extrapolation from the edge measurement of XRF to the entire assembly.

Given the low energy of the x-rays relative to the rest of the spectrum coming from spent fuel, essentially the only way to reduce the count rate to a level that the detection system can handle is to collimate. Scanning the collimator values in Table 3 we see that the values range from 1 to 3 mm with the vast majority of the more realistic inspection cases having a radius of 2 mm or less; the 1 mm radius would result in a ~3 mm^2 projected collection area on the fuel. Therefore, combining the observed surface area with the fact that the mean free path of a 100 keV photon is around 0.5 mm, we can conclude that the majority of the signal obtained from a single detector in an XRF system will obtain its signal from a volume in the fuel of 1 to 20 mm^3. This is an important number since it quantifies the task of extrapolating from edge measurements to the whole of the assembly.

4.8 Pu Profile

Symmetry from the infinite boundary condition used in the SFL creation is partially responsible for the excellent agreement between the simulated XRF Pu/U ratios and the Pu/U mass calculated in the assembly. Preliminary work in creating the second SFL mentioned previously was used to produce Figure 24, which gives the Pu mass in the outer ring of pins for a 45 Gwd/tU BU, 4% IE, and 5 year CT. For this example, the Pu mass on one face of the assembly is about 10% less than another face. The effects of asymmetric Pu distribution and the general problem of Pu extrapolation from the measured front pins is left for future work.

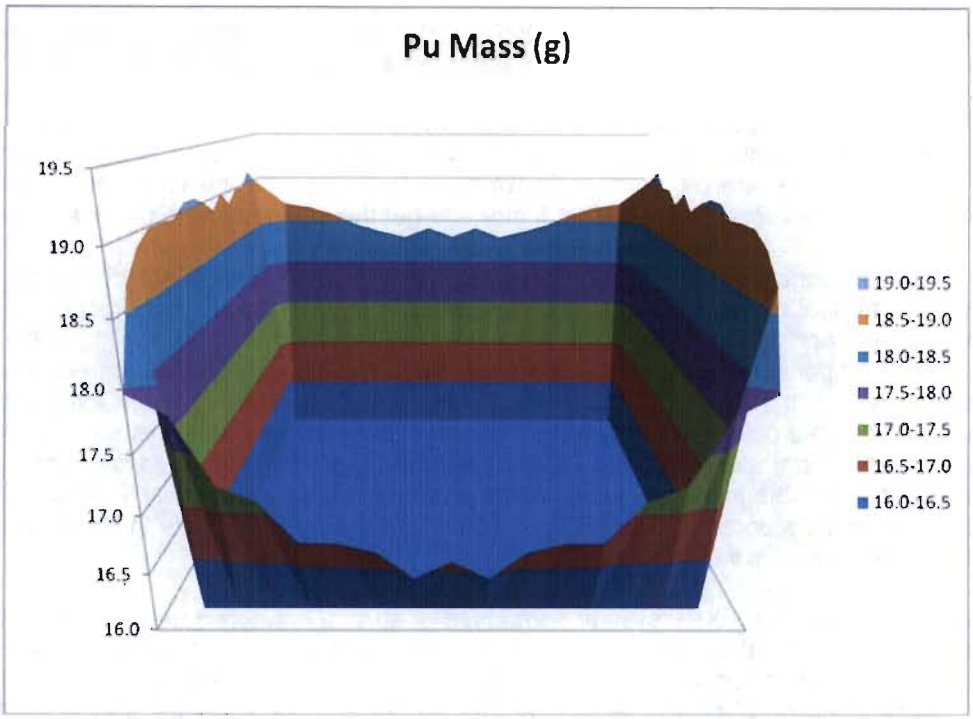

Figure 24: The Pu mass in the outer ring of pins for an assembly with 45 Gwd/tU BU, 4% IE, and 5 year CT.

5. Conclusion

An XRF measurement of a spent fuel rod section, labeled 649C, made at ORNL was simulated to determine our capability to model XRF signals. Modeling of XRF signatures in spent fuel with MCNPX presents many challenge because of the heavy collimation needed to suppress the high photon field. Breaking the problem into two separate MCNPX calculations made the simulation possible with available resources. Modeling of the 649C fuel pin suggest that the beta emission in spent fuel accounts for roughly 10% of the XRF signal. The magnitude of the 649C simulation spectrum was off by an order of magnitude; however, the Pu/U ratio simulated is in good agreement with the Pu/U ratio measured; suggesting a normalization problem. The Pu/U ratio simulated differed from the measurement by 2.65%, which is within 3 sigmas of the measured data. Successful modeling of the Pu/U ratio for a single fuel pin, gave us confidence in our ability to model XRF signals from spent fuel.

Modeling of the spent fuel library indicated that despite the low penetrability of x-rays in spent fuel, it should be possible to observe measurable Pu x-ray peaks. Furthermore, across the suite of different BUs, IEs, and CTs simulated, the XRF Pu/U ratio had a very strong correlation with the Pu/U mass ratio present in the fuel, suggesting that XRF is a feasible technique for quantifying Pu in spent nuclear fuel. Uncertainty in the Pu/U ratio from counting statistics varied greatly between assemblies because of the variation in the gamma intensities that primarily drive the XRF signal. Choosing the collimator radius to correct for different source intensities, a single detector with a 1 hour count time can expect approximately 10% uncertainty. A 10 hour count time corresponded to roughly a 4% uncertainty in the Pu/U ratio.

The spent fuel assemblies used in the simulation were created using an assumption of symmetry that is not representative of real world reactor loading plans, where different sides of an assembly can have very different BUs, and thus, different Pu masses. Given that the low penetrability of x-rays in fuel means that XRF is only measuring the outermost pin in an assembly, the ability with which one can accurately extrapolate the Pu profile from the edge to the entire assembly is the key issue in assessing the utility of XRFs for quantifying Pu mass in a full assembly. Future work with assemblies that do not have symmetrical BUs is needed to examine the effect this will have on XRFs feasibility as an assay technique for spent fuel assemblies.

6. Acknowledgments

The authors would like to acknowledge the support of the Next Generation Safeguards Initiative Office of Nuclear Safeguards & Security (NA-241) National Nuclear Security Administration U.S. Department of Energy

7. References

1. Scheinman, Next Generation Safeguards Initiative Inaugural Conference, September 11-12, 2008. Available at: http://nnsa.energy.gov/nuclear_nonproliferation/2147.htm.

2. Tobin, S. J., Sandoval, N. P., Fensin, M. L., Lee, S. Y., Ludewigt, B. A., Menlove, H. O., Quiter, B. J., Rajasingum, A., Schear, M. A., Smith, L. E., Swinhoe, M. T., Thompson, S. J., *Determination of Plutonium Content in Spent Fuel with Nondestructive Assay*, Annual Meeting of the Institute of Nuclear Material Management, Tuscon, AZ, 2009.

3. Reilly, D., Ensslin, N., Smith, H. (Jr), et al. *Passive Nondestructive Assay of Nuclear Materials*, United States Nuclear Regulatory Commission. NUREG/GR-5550. March 1991.

4. Rudy, *Determination of Pu in Spent Fuel Assemblies by X-Ray Fluorescence*, Institute of Nuclear Material management Annual Conference," 2005.

5. Charlton, W., et. al., *The Use of Self-Induced XRF to Quantify the Pu Content in PWR Spent Nuclear Fuel*, Proceedings of the 31st Annual Conference of the ESARDA, Vilnius, Lithuania, May 2009, European Safeguards Research and Development Association.

6. *MCNPX User's Manual*, Version 2.6.0. Los Alamos National Laboratory, April 2008. Available at: https://mcnpx.lanl.gov/.

7. V. Mozin, S. Tobin, J. Vujic, *Delayed Gamma Instrument for Determining Plutonium Mass in Spent Nuclear Fuel*, Proceedings of the 2010 ANS annual meeting, San Diego, California, 2010.

8. V. Mozin, et. al., *Delayed Gamma Technique for Fissile Material Assay*, Proceedings of the 51st Annual Meeting of the INMM, Baltimore, Maryland, 2010.

9. Wilson, W. B., et. al., *A Manual for CINDER'90 Version 07.4 Codes and Data*, Los Alamos National Laboratory Report, 2008.

10. *WWW Table of Radioactive Isotopes*, Ernest O. Lawrence Berkeley National Laboratory and Lund University, Sweden. Available at: http://ie.lbl.gov/toi/index.asp, 2004.

11. Fensin, M. L., *MCNPX Memory Reduction Patch-FY 2009*, Los Alamos National Laboratory Report, 2009.

12. Trellue, H., Frensin, M., Richard, J., Galloway, J., Conlin, J., *Description of the Spent Nuclear Fuel Used in the Next Generation Safeguards Initiative to Determine Plutonium Mass in Spent Fuel*, Los Alamos National Laboratory Report, 2010.